Journal of Applied Research in Water and Wastewater
E-ISSN: 2476-6283
Journal homepage: https://arww.razi.ac.ir

Evaluation of the various adsorption isotherm models for the photocatalytic removal of methylene blue from the wastewater by graphene oxide/TiO_2/SiO_2

Seyed Mehdi Sajjadi*

Department of chemical Engineering, Faculty of Engineering, University of Bonab, Bonab, Iran.

GRAPHICAL ABSTRACT

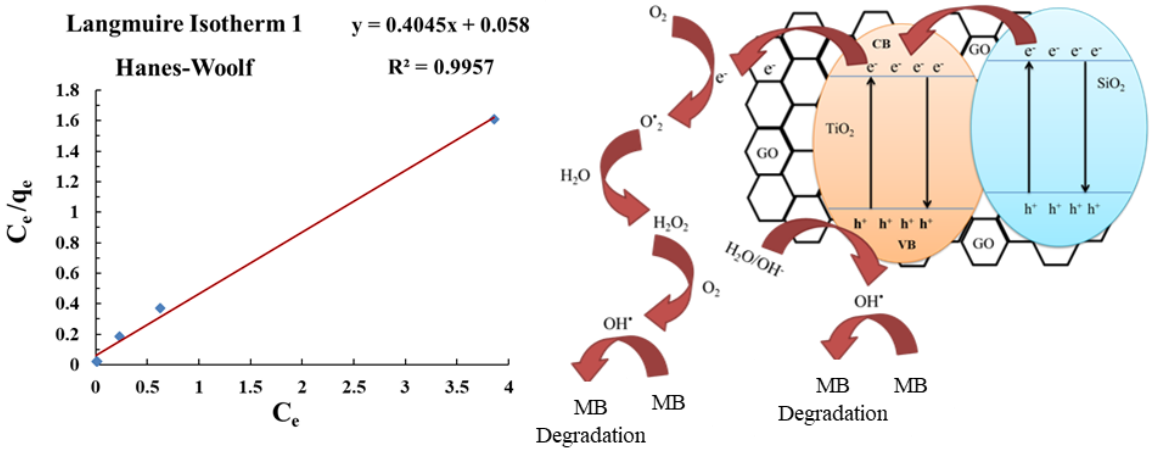

ARTICLE INFO

Article type:
Research Article

Article history:
Received 1 January 2024
Received in revised form 5 March 2024
Accepted 6 March 2024
Available online 7 March 2024

Keywords:
Graphene oxide/TiO_2/SiO_2 photocatalyst
Methylene blue
Wastewater
Isotherms

ABSTRACT

Treatment of wastewater is a crucial step in reducing pollution from the textile and dyeing industries. One of the best techniques for dye removal is photocatalytic processes, and TiO_2 is frequently employed in numerous wastewater treatment applications. In this study, different adsorption isotherm models and experimental data from the removal of the methylene blue dye from wastewater by applying GO/TiO_2/SiO_2 nanocomposite were compared. The correlation coefficient values (R^2) for the Langmuir isotherm type 1 (Hanes-Woolf), Temkin, and Freundlich were determined to be, respectively, 0.9957, 0.9823, and 0.9515. Additionally, the R^2 values for the Redlich-Peterson, Sips, and Toth isotherms models were 0.9575, 0.9626, and 0.9629, respectively. Therefore, Langmuir isotherm type 1 has the highest R^2 and is the best model for surface adsorption of methylene blue on GO/TiO_2/SiO_2 photocatalyst. As a result, monolayer adsorption was most likely dominating during the adsorption. Furthermore, this photocatalyst proved suitable for lower methylene blue concentrations and systems with lower temperature sensitivity.

1. Introduction

Protecting the environment against pollution created by contemporary industries and technologies, which endangers public health, is one of humanity's present concerns (Liu *et al.*, 2009; Periyasamy *et al.*, 2023; Sajjadi and Haghighi, 2018). The discharge of colored and non-colored effluents from a variety of industries, including textiles, paper, cosmetics, agriculture, plastics, and leather, causes serious environmental problems (Jegannathan and Nielsen, 2013; Manojkumar *et al.*, 2023). Because some dyes are poisonous, presence of them not only damages beautiful natural landscapes but also damages aquatic ecosystems (Singh, Singh and Singh, 2015; Cao *et al.*, 2019). Recently, industries have come under great pressure from government officials and the general public to cleanse wastewater before it is dumped into the environment. As a result, developing effective treatment approaches is both required and unavoidable. According to studies, approximately 12% of the dye used in the textile sector enters the effluent and approximately 20% of this quantity, combined with the treated effluent, returns to nature (Pei *et al.*, 2017). Various approaches are utilized to separate hazardous colors that constitute a major harm to nature and the environment, including chemical methods, physical methods, and biological methods (Bustos-Terrones *et al.*, 2021). It should be noted that dye separation is difficult due to the dyes' solubility in water. As a result, extensive research was conducted in order to develop an efficient and cost-effective system for the treatment of colored effluents. To get rid of non-biodegradable and extremely stable

*Corresponding author Email: seyedmehdi_sajjadi@yahoo.com
Mehdi_sajjadi@ubonab.ac.ir

Cite this article: S.M. Sajjadi, Evaluation of the various adsorption isotherm models for the photocatalytic removal of methylene blue from the wastewater by graphene oxide/TiO_2/SiO_2, *Journal of Applied Research in Water and Wastewater*, 11 (1), 2024, 59-66. doi: https://doi.org/10.22126/arww.2023.8980.1286

substances in water, advanced oxidation processes (AOPs), which fall under the category of chemical techniques, have recently undergone substantial research. In fact, AOP techniques would use highly reactive species produced on-site, like $^{\bullet}OH$ and $^{\bullet}O_2$ radicals. These radicals quickly oxidize the pollutants, turning them into CO_2, H_2O, or small inorganic ions (Ge *et al.*, 2019; Zarrabi, Haghighi and Alizadeh, 2018; Hosseinzadeh *et al.*, 2023). For the treatment of contaminated water, advanced oxidation technologies such the Fenton process, photo-Fenton process, ozonation process, and photocatalytic approach are used. Compared to other methods, photocatalytic processes are more promising tools for wastewater dye degradation (Ncibi, Mahjoub and Seffen, 2007; Rabanimehr *et al.*, 2021; Chiani *et al.*, 2020). Recent research have looked into the use of nanoparticles as photocatalysts as an environmentally friendly technique that could improve wastewater remediation. TiO_2 photocatalyst has attracted increased attention in this area of research because of its affordability, non-toxicity, fast reactions, and high-efficiency capacity to absorb pollutants and remove dye from contaminated water (Ge *et al.*, 2019; Kong *et al.*, 2022; Chakraborty *et al.*, 2022). The particle size of TiO_2 plays a crucial role in determining the physical and chemical properties of photocatalysts. As a result, a considerable number of studies have been conducted by various researchers to explore the correlation between particle size and synthesis techniques of photocatalysts (Bakardjieva *et al.*, 2006).The sol-gel method has been extensively employed in the production of nanocatalysts owing to its capability to operate at low temperatures and its capacity to control particle size and morphology (Sajjadi, Haghighi and Eshghi, 2019; Riazian and Bahari, 2012; Sajjadi and Haghighi, 2019; Shokrolahi, Farhadian and Davari, 2019). Nevertheless, TiO_2 exhibits suitability as a potential candidate for the degradation of dyes through photocatalysts. Nonetheless, certain significant limitations persist. TiO_2 is a photocatalyst with a high-energy band gap, necessitating a significant input of energy for its activation. The wavelength associated with the specified energy should not exceed 385 nm. The utilisation of sunlight energy for photoreactions is effectively precluded by this constraint. Furthermore, a diminished rate of electron transfer to oxygen and an elevated rate of electron-hole recombination in an excited state, lead to a reduced quantum yield rate and a constrained photo-oxidation rate (Tseng *et al.*, 2009). Furthermore, empirical investigations have demonstrated that the incorporation of a reduced quantity of SiO_2 into TiO_2 enhances its photocatalytic efficacy as a result of improved thermal stability and increased surface area (Riazian, 2014; Rosales and Esquivel, 2020). Moreover, the combination of TiO_2 with graphene oxide (GO) has demonstrated improved photocatalytic activity in comparison with the neat TiO_2. The prevailing consensus in the scientific community is that graphene sheets serve as electron acceptors, hence facilitating the transfer and separation of photogenerated electrons during the excitation of TiO_2. This process effectively diminishes the recombination of electron-hole pairs (Li *et al.*, 2016; Lu *et al.*, 2021).Thus, it was deduced that the GO/SiO_2 modified TiO_2 nanocomposite exhibited favorable characteristics as a photocatalyst in degradation of methylene blue.

In order to comprehend the adsorption mechanisms within the aforementioned photocatalyst, it is imperative to acquire equilibrium data, which is generally referred to as adsorption isotherms. The characterization of adsorption isotherms holds significant importance in elucidating the nature of interactions between adsorbate molecules or ions and the adsorption sites present on the surface. Therefore, it is crucial to establish the link between equilibrium data by the utilisation of either a theoretical or empirical equation in order to facilitate the understanding and forecasting of adsorption phenomena. An adsorption isotherm refers to a mathematical equation that describes the correlation among the quantity of solute adsorbed on the adsorbent and concentration of solute in the liquid phase. The significance of adsorption is rooted in its ability to elucidate the nature of the interaction between an adsorbate and an adsorbent, hence playing a pivotal role in the development and optimisation of adsorption processes. Numerous equilibrium models were created to elucidate the correlation between isotherms in a state of equilibrium (Demiral and Güngör, 2016).

The isotherm data in this study was assessed by employing various isotherm equations, like Langmuir, Freundlich, Temkin, Redlich-Peterson, Sips, and Toth. Based on the findings of this inquiry, it can be inferred that the adsorption process occurred in either a monolayer or a multilayer configuration. Moreover, the synthesised $GO/TiO_2/SiO_2$ photocatalyst shown suitability for both higher and lower concentrations of adsorbent. Moreover, it is worth considering whether the aforementioned photocatalyst is suitable for systems that are sensitive to temperature. It can be argued that the use of extracted data in future synthesis processes, results in reduced costs, decreased time requirements, and improved outcomes.

2. Experimental

The present investigation was conducted utilising the findings of other investigations (Alahmad *et al.*, 2018; Ahmad and Alahmad, 2021), as previously indicated. Hence, in order to ensure a thorough investigation and adequate elucidation of the used methods and analyses, the initial synthesis procedure of $GO/TiO_2/SiO_2$ nanoparticles, as reported by Alahmad and coworkers (Alahmad *et al.*, 2018), was introduced. The synthesis of $GO/TiO_2/SiO_2$ nanoparticles was conducted by sol-gel method. The weight percentages of synthesised nanocatalysts were provided in Table 1.

Table 1. Weight percentages of the synthesized $GO/TiO_2/SiO_2$ nanoparticles (Ahmad and Alahmad, 2021).

Catalyst type	GO, %	Ti, %	Si, %
$GO/TiO_2/SiO_2$	0.966	24.15	74.9

Next, 0.15 g of $GO/TiO_2/SiO_2$ nanoparticles was introduced into the solutions containing varying concentrations of methylene blue dyes. The concentrations of dye utilized in experiment were as follows: 0.5, 1, 3, 5 and 10 ppm. Cited concentrations were denoted as initial concentrations. Furthermore, it should be noted that the pH value was consistently maintained at 6 in all of the solutions. Afterward, while the solution was mixed, dye degradation test was conducted under the influence of UV lamp for each individual solution. Sampling was conducted at regular 30 min intervals, followed by the measurement of methylene blue absorbance using a UV-Vis spectrophotometer (Ahmad and Alahmad, 2021). Afterward, while the solution was mixed, dye degradation test under the UV lamp was done for each solution. At an interval of each 30 min, sampling was done and then absorbance of methylene blue was measured on UV-Vis spectrophotometer (Ahmad and Alahmad, 2021). Next, a diagram of methylene blue degradation versus initial concentration was depicted. The provided diagram is represented as Fig. 1. The diagram was acquired under conditions of constant temperature and is referred to as the isotherm equation.

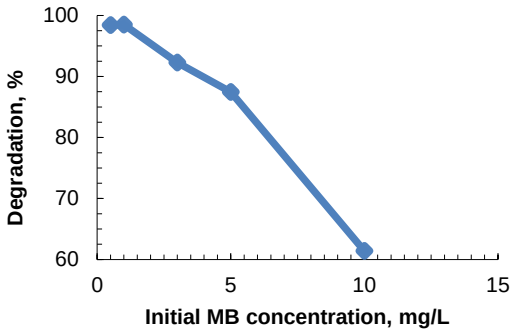

Fig. 1. Degradation percentage of methylene blue at different initial concentrations (Alahmad *et al.*, 2018).

In addition to the diagram derived from the experimental data, there are numerous mathematical-based diagrams, like Langmuir, Freundlich, Temkin, Redlich-Peterson, Sips, and Toth isotherms. These mathematical equations and formulas have the capability to forecast the degradation of dye in relation to concentration which is called adsorption isotherm. The Freundlich, Langmuir, and Temkin isotherms are two-parameter isotherms, whereas the Redlich-Peterson, Sips, and Toth models are three-parameter models. We conducted an investigation to determine the isotherm that exhibited the highest accuracy in predicting the experimental outcomes, as measured by the lowest error. The identification of an appropriate isotherm for each nanoparticles enables the estimation of trends in dye degradation across various solution concentrations. This section will provide concise explanations regarding the aforementioned isotherms.

Langmuir Isotherm

The Langmuir isotherm was developed considering the equilibrium between the rates of adsorption and desorption processes. Owing to this isotherm, adsorption takes place over the homogeneous surface. Also, adsorption energy is constant for all sites. Moreover, once molecule attaches a site, no additional adsorption is not possible there (Osmari *et al.*, 2013). In addition, this model assumes a monolayer coverage of the adsorption surface and also is suitable for lower concentrations of adsorbent. Langmuir isotherm was demonstrated in Eq. (1) (Dada *et al.*, 2012).

$$q_e = \left(\frac{q_m K_L C_e}{1 + K_L C_e}\right) \quad (1)$$

where, q_e (mg/g) and q_m (mg/g) indicate the milligram of absorbed per gram of the adsorbent and maximum adsorption capability of adsorbent, correspondingly. Also, K_L is Langmuir constant ($L.mol^{-1}$). Generally, three linear forms of Langmuir isotherm were reported in literature (Osmari *et al.*, 2013). These are as follows: Langmuir isotherm type 1(Hanes-Woolf), Langmuir isotherm type 2 (Lineweaver-Burk) and also, Langmuir isotherm type 3 (Eadie- Hofstee) which were presented in Table 2 in Eqs. 2-4, respectively.

Table 2. Various linear forms of the Langmuir isotherms.

$\frac{C_e}{q_e} = \frac{1}{q_m K_L} + \frac{C_e}{q_m}$	Langmuir Isotherm 1 (Hanes - Woolf)	(2)
$\frac{1}{q_e} = \frac{1}{q_m} + \left(\frac{1}{q_m K_L}\frac{1}{C_e}\right)$	Langmuir Isotherm 2 (Lineweaver-Burk)	(3)
$q_e = q_m - \frac{1}{K_L}\frac{q_e}{C_e}$	Langmuir Isotherm 3 (Eadie – Hofstee)	(4)

The values of q_m and K_L for each isotherm need to be derived from separate plots, as illustrated by the equations mentioned above (Osmari *et al.*, 2013).

Freundlich Isotherm

The Freundlich isotherm was the initial adsorption equation that was introduced. This isotherm has commonly been utilized as an empirical equation to characterize adsorption on heterogeneous surfaces. During the investigation of adsorption with Freundlich isotherm, it must be noted that for the dilute concentrations, Henry's law is not accurate. Moreover, Freundlich isotherm is appropriate for multiplayer adsorption and also, is proper for high and middle range of absorbent concentration. So, there are some differences between Langmuir and Freundlich isotherms (Dada *et al.*, 2012; Osmari *et al.*, 2013). The Freundlich isotherm is as follows:

$$q_e = K_F C_e^{\left(\frac{1}{n}\right)} \quad (5)$$

The Freundlich isotherm in its linear form, which will be employed for our computations, is given by:

$$\ln(q_e) = \ln(K_F) + \frac{1}{n}(\ln C_e) \qquad \ln q_e \text{ vs } \ln C_e \quad (6)$$

Where, K_F is the presentation of adsorption capacity. Additionally, the function $\frac{1}{n}$ can be attributed to the adsorption strength. The $\frac{1}{n}$ values indicate the nature of the isotherm as irreversible($\frac{1}{n} = 0$), satisfactory and normal adsorption ($0 < \frac{1}{n} < 1$), and unfavorable ($\frac{1}{n} > 1$) (Dada *et al.*, 2012; Osmari *et al.*, 2013).

Temkin Isotherm

Temkin isotherm includes a parameter that obviously considers the interactions which are between the adsorbent and adsorbate. Owing to the Temkin isotherm, intensifying the coverage rate on the adsorbent surface leads to the lower adsorption heat of molecules. Also, adsorption is determined with homogeneous spread of binding energies, as far as a maximum binding energy (Dada *et al.*, 2012; Osmari *et al.*, 2013; Chu, 2021). Moreover, Temkin isotherm investigates the influence of temperature adsorption that declines linearly with coverage of adsorbate and adsorbent. Temkin isotherm is as follows:

$$q_e = \frac{RT}{b}\ln(K_T) + \frac{RT}{b}(\ln C_e) \qquad q_e \text{ vs } \ln C_e \quad (7)$$

The equilibrium binding constant, denoted as K_T, is expressed in units of L/mol. The constant "b" in the Temkin isotherm equation represents the adsorption heat. The universal gas constant, denoted as R, has a value of 8.314 J/mol.K. In given context, T represents the temperature in Kelvin (K). Moreover, slope of the function can be denoted as RT/b, while the intercept can be represented as the product of RT/b and the natural logarithm of K_T. (Dada *et al.*, 2012; Osmari *et al.*, 2013; Chu, 2021).

Redlich-Peterson Isotherm

The Redlich-Peterson model is a three-parameter model that integrates the parameters of Langmuir and Freundlich isotherms. So, the adsorption process is able to exhibit both homogeneous and heterogeneous characteristics. The Redlich-Peterson isotherm can be expressed as:

$$q_e = \frac{K_R C_e}{1 + \alpha_R C_e^{\beta}} \quad (8)$$

Where, K_R ($L\ g^{-1}$) and α_R ($mg\ L^{-1})^{-\beta}$ are Redlich-Peterson constants. Also, β (dimensionless) parameter takes values from 0 to 1 (Shikuku and Jemutai-Kimosop, 2020).

Sips Isotherm

The Sips isotherm, which is a three-parameter model, integrates elements of Freundlich and Langmuir isotherms. This model is appropriate for heterogeneous systems where adsorbed molecule can take up more than one binding site. Sips isotherm equation is given by:

$$q_e = \frac{q_m a_s C_e^{B_S}}{1 + a_s C_e^{B_S}} \quad (9)$$

Where, q_m, a_s and B_s are the constants. Moreover, B_s represents the heterogeneity index. In general, it may be stated that a higher value of B_s indicates a greater degree of heterogeneity within the system. On the contrary, values that approach unity indicate a uniform adsorbent surface that aligns with the principles of the Langmuir equation (Shikuku and Jemutai-Kimosop, 2020).

Toth Isotherm

The Toth isotherm (Eq. 10) enhances the accuracy of Langmuir isotherm to equilibrium data for both low and high adsorption concentrations.

$$q_e = \frac{q_m C_e}{(a_T + C_e^{\,z})^{\frac{1}{z}}} \quad (10)$$

Parameter a_T is the Toth model constant. The heterogeneity of the system is characterized by the temperature-independent parameter z. The degree of heterogeneity is proportional to how far it is from unity (Shikuku and Jemutai-Kimosop, 2020).

The process of fitting experimental data with the aforementioned isotherms provides valuable insights into the specific characteristics of the adsorbing system. Hence, by conducting a comparative analysis between the experimental data of the GO/TiO_2/SiO_2 photocatalyst and different models, valuable insights can be gained regarding the underlying mechanism. This information can further aid in the development of novel adsorption systems tailored for the efficient degradation of diverse wastewater pollutants, including methylene blue. The primary objective of this investigation was to identify a suitable adsorption isotherm for the removal of methylene blue using the GO/TiO_2/SiO_2 photocatalyst. The experimental data utilized in this study was obtained from reputable literature sources (Alahmad *et al.*, 2018; Ahmad and Alahmad, 2021) and afterwards compared with several adsorption isotherm models. Experimental data which were applied for comparison were presented in Table 3 (Alahmad *et al.*, 2018; Ahmad and Alahmad, 2021). The quantity of dye adsorbed at equilibrium, denoted as qe (mg/g), might be determined using Eq. 11:

$$q_e = (C_0 - C_e) * \left(\frac{V}{W}\right) \quad (11)$$

In Eq. 11, C_0 (mg/L) and C_e (mg/L) were the first concentration and the final concentration of dye, respectively. Moreover, V (l) and W (g) were solution volume and adsorbent weight, respectively (Dada *et al.*, 2012; Abdoli, Bastani and Bargozin, 2015).

Table 3. Experimental data of Methylene Blue degradation which were extracted from literature (Ahmad and Alahmad, 2021)

C_0	C_e	q_e	ln (C_e)	ln(q_e)	C_e/q_e	q_e/C_e
0.5	0.0079	0.35	-4.8409	-1.0498	0.0226	44.3038
1	0.0149	0.65	-4.2064	-0.4308	0.0229	43.6241
3	0.2316	1.25	-1.4627	0.2231	0.1853	5.3972
5	0.6275	1.7	-0.4660	0.5306	0.3691	2.7092
10	3.8601	2.4	1.3507	0.8755	1.6083	0.6218

3. Results and discussions

3.1. Characterizations of GO/TiO_2/SiO_2 photocatalyst

This part begins by presenting the outcomes of several characterizations conducted on the prepared nanocatalysts, including

XRD, SEM and FTIR analyses. Owing to the XRD patterns (Fig. 2) some peaks were detected at 2θ= 25.3°, 37.8°, 48°, 54°, 55.1°, and 62.7° which were belong to anatase phase. No characteristic peaks for Si and C were found. This could be attributed to the high crystallinity of anatase phases and significant intensity of peaks (Alahmad *et al.*, 2018).

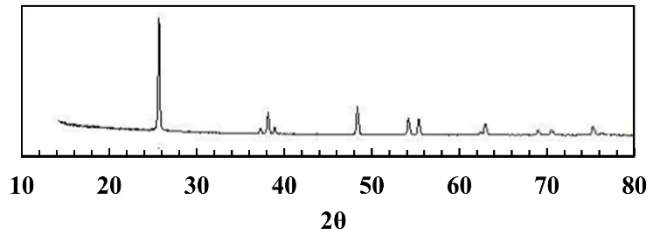

Fig. 2. XRD patterns of GO/TiO_2/SiO_2 photocatalyst (Alahmad *et al.*, 2018).

Results of FTIR analysis of GO/TiO_2/SiO_2 photocatalyst were exhibited in Fig. 3. The peaks between 736 and 742 cm^{-1} were assigned to the Ti-O bonds. The peak at 942 cm^{-1} was correspond to the Ti-O-Ti bond. The absorption peak at 1083 cm^{-1} was attributed to the O-Si bond. The peaks at 3359.9 and 1628 cm^{-1} were ascribed to the OH groups. (Alahmad *et al.*, 2018; Sajjadi *et al.*, 2022).

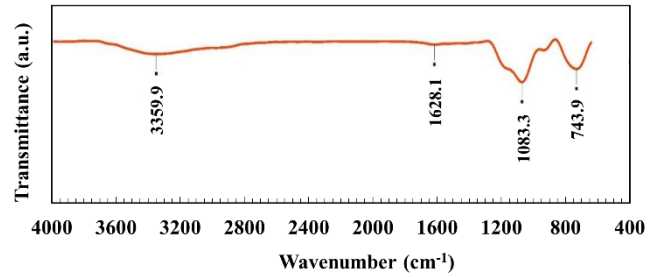

Fig. 3. FTIR analysis of GO/TiO_2/SiO_2 photocatalyst (Alahmad *et al.*, 2018).

The morphology of photocatalysts was assessed by SEM analysis and illustrated in Fig. 4. Approximately uniform morphology with spherical particles was obtained. Also, in some points of images, sheet-like morphology were found which were belong to GO sheets (Alahmad *et al.*, 2018).

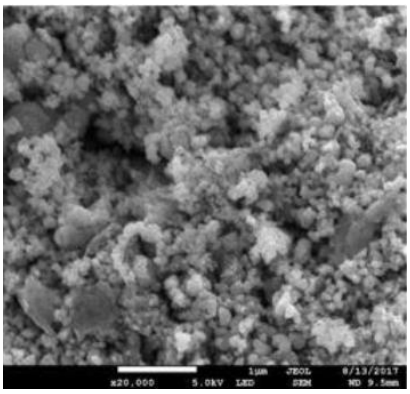

Fig. 4. SEM images of GO/TiO_2/SiO_2 photocatalyst (Alahmad *et al.*, 2018).

In this section, experimental data (methylene blue dye degradation results) were compared with various isotherm models such as the Langmuir isotherm model (three different types), Freundlich, Temkin, Redlich-Peterson, Sips and Toth isotherms.

3.2. Comparing with Langmuir Isotherms

In this section, experimental data about the adsorption of methylene blue dye by applying of GO/TiO_2/SiO_2 nanoparticles and utilization of different types of Langmuir isotherm models were tested. Experimental data which were applied for the comparison were given in Table 3. The results of the evaluation for Langmuir isotherm type 1 (Hanes-Woolf), Langmuir isotherm type 2 (Lineweaver-Burk) and Langmuir isotherm type 3 (Eadie- Hofstee) were represented in Figs. 5-7, respectively. The constants and parameters of the models were listed along with the correlation coefficient values in Table 4. Owing to the calculated data in Table 4, for Langmuir isotherm type 1 (Hanes- Woolf), Langmuir isotherm type 2 (Lineweaver-Burk) and Langmuir isotherm type 3 (Eadie- Hofstee), R^2 were 0.9957, 0.9770 and 0.7963, respectively. Hence, it can be shown that Langmuir isotherm type 1 exhibited a greater degree of compatibility with the experimental data in comparison to the other forms of Langmuir isotherms.

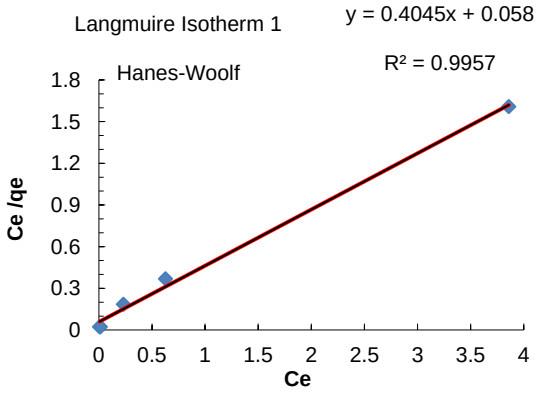

Fig. 5. Comparing of Methylene blue's anticipated and observed adsorption results with regarding to Langmuir isotherm type 1.

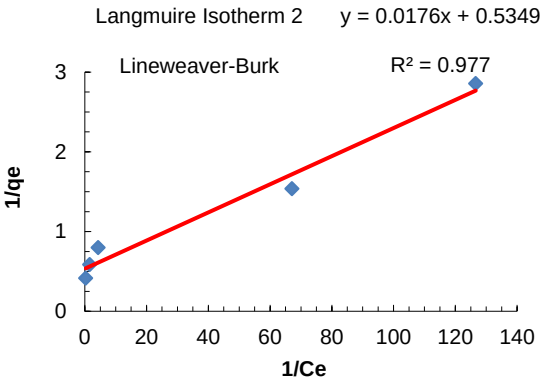

Fig. 6. Comparing of Methylene blue's anticipated and observed adsorption results with regarding to Langmuir isotherm type 2.

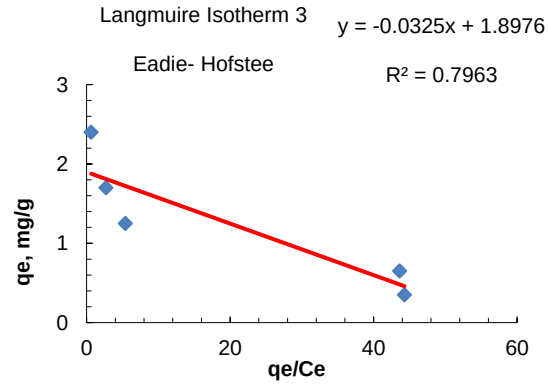

Fig. 7. Comparing of Methylene blue's anticipated and observed adsorption results with regarding to Langmuir isotherm type 3.

Table 4. Parameters of Langmuir isotherms which were obtained from the calculations.

Langmuir Isotherm type	q_m, mg/g	K_L, l/mg	R^2
Type 1	2.4722	6.9741	0.9957
Type 2	1.8695	30.3921	0.9770
Type 3	1.8976	30.7692	0.7963

To clarify the difference between the linear forms of the Langmuir isotherm, Addition of some statement regarding to their nature is beneficial. The Langmuir isotherm type 3, also known as the Eadie-Hofstee isotherm, incorporates the reciprocal of the qe and Ce variables in the regression analysis. This approach often results in regression difficulties primarily influenced by low q_e and C_e values, which are typically measured with poorer accuracy. Furthermore, while it is reasonable to assume that the variances of q_e and C_e remain constant

within the experimental range under analysis, it is not reasonable to make the same assumption for the reciprocals of these variables. The aforementioned observation can be easily extrapolated to the other linear variations of the Langmuir isotherm. It is important to note that the Langmuir isotherm type 2 (Lineweaver-Burk) use the variable q_e to define both the independent and dependent variables. This dual usage of q_e may result in contradictory definitions of measurement fluctuations. The Langmuir isotherm type 1, also known as the Hanes-Woolf isotherm, employs the variable C_e to represent both the independent and dependent variables in its description. The model formulation possesses a distinctive quality that has the potential to artificially induce a strong correlation between the independent and dependent variables. So, model predictions exhibit a high correlation with the experimental data. Hence, the graphical representation of C_e/q_e as a function of C_e yielded a highly effective model that accurately corresponds to the empirical observations, thereby commonly being chosen as the optimal linear model of the Langmuir isotherm (Osmari *et al.*, 2013; Parimal, Prasad and Bhaskar, 2010).

To ascertain the favourability or unfavourability of methylene blue adsorption by the GO/TiO_2/SiO_2 photocatalyst in relation to the Langmuir type adsorption process, the shape of the isotherm can be characterised using the dimensionless parameter referred to as the separation factor (R_L). This can be achieved by employing the following Eq.

$$R_L = \frac{1}{1 + K_L C_0} \quad (12)$$

K_L (L/mol) and C_0 (mol/L) are the Langmuir constant and initial concentration of dye, respectively. Calculated R_L defines the state of adsorption. R_L = 0 and 1 indicate that adsorption is irreversible and linear, respectively. 0<R_L<1 is ascribed to favorable adsorption. Finally, R_L >1 shows unfavorable adsorption (Safri and Fletcher, 2023). As shown in Table 5, for all C_0, calculated R_L was in the range of 0 and 1. Therefore, adsorption was favorable.

Table 5. Separation factor for methylene blue adsorption on GO/TiO_2/SiO_2 photocatalyst.

Initial concentration, mg/L	R_L for Langmuir type 1	R_L for Langmuir type 2	R_L for Langmuir type 3
0.5	0.2229	0.0617	0.0610
1	0.1254	0.0319	0.0314
3	0.0456	0.0108	0.0107
5	0.0278	0.0065	0.0065
10	0.0141	0.0033	0.0032

The R_L values for all models were within the range of 0 to 1. The values of R_L for Langmuir isotherm types 2 and 3 were comparatively lower than those for type 1 and exhibited a closer proximity to zero. As previously mentioned, the process of adsorption is deemed irreversible when the value of the Langmuir adsorption equilibrium constant (R_L) is equal to zero. It can be concluded that the behaviour exhibited by Langmuir isotherms of types 2 and 3 closely resembled that of the irreversible type. However, owing to the R^2 values, it can be concluded that Langmuir isotherm type 1 was more favorable. Based on the observed lower R_L values, approaching zero, for Langmuir isotherm types 2 and 3 (irreversible type), as well as the higher R^2 value for Langmuir isotherm type 1, it can be inferred that the Langmuir isotherm type 1 is more favorable when compared to the other types of Langmuir isotherms.

3.3. Comparing with Freundlich Isotherm

Fig. 8 demonstrates the validation of the experimental data (Table 3) using the Freundlich isotherm for adsorption of methylene blue by the GO/TiO_2/SiO_2 photocatalyst. The constant, parameters, and correlation coefficient value of this isotherm were documented in Table 5. Due to the calculations performed, R^2 for Freundlich isotherm was determined to be 0.9515, indicating a lower value compared to both types 1 and 2 of the Langmuir isotherms.

Table 5. Parameters of Freundlich isotherm which was obtained from calculations.

n	K_F, mg/g	R^2
3.4376	1.8034	0.9515

Upon comparing the correlation coefficient values associated with Langmuir and Freundlich isotherms, it was revealed that the Langmuir isotherm exhibited a superior fitting to the adsorption data in comparison to the Freundlich isotherm. Adsorption, according to the Langmuir model, takes place as a monolayer of adsorbate molecules over the uniform adsorbent surface. Therefore, better performance of the Langmuir probably originated from the monolayer nature of adsorption.

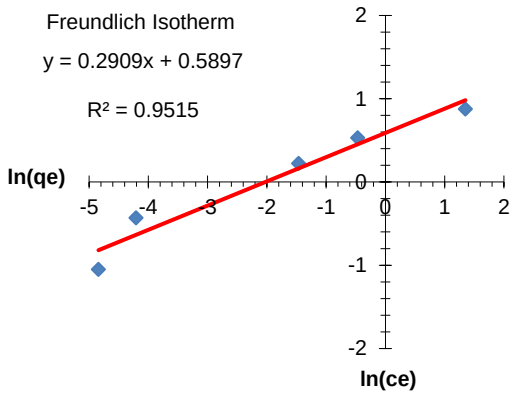

Fig. 8. Freundlich isotherm performance for removing of the methylene blue dye.

To evaluate the monolayer adsorption, dimensions of methylene blue is required. It has been documented that the width, length and thickness of methylene blue were 1.43, 0.61, and 0.4 nm, respectively. As well, calculation of q_D (monolayer adsorption capacity) is necessary. Computation of q_D is possible with applying of Eq. 13.

$$q_D = \frac{(S_{BET}/(1.43 * 0.61 * 10^{-18}))}{N_A} * (M) \quad (13)$$

In Eq. 13, N_A = 6.02 ×10^{23} mol^{-1} is the Avogadro's constant. Moreover, M is the molecular weight of methylene blue (319.85 g/mol). In addition, S_{BET} is the specific surface area (Wang *et al.*, 2019; Vargas *et al.*, 2011). Also, q_m was the maximum adsorption capacity. If $q_m > q_D$ we can conclude that multilayer adsorption takes place, but if $q_m < q_D$ monolayer adsorption is possible. It must be noted that applied method for the synthesis of photocatalysts was the sol-gel method. This method is one of the appropriate methods which is able to produce materials with higher surface area. Owing to the obtained data from Alahmad and co-workers (Alahmad *et al.*, 2018; Ahmad and Alahmad, 2021) and other studies (Mungondori and Tichagwa, 2013; Joseph *et al.*, 2021) it is more probable that q_D is larger than q_m and thus monolayer adsorption was dominant. Therefore, it is reasonable and acceptable to conclude that the Langmuir isotherm provides a more accurate match for adsorption data in comparison with the Freundlich isotherm.

Furthermore, the value of n was 3.4376 and consequently 1/n was 0.2901. So, adsorption was normal and also, Freundlich model was proper for this adsorption. But in order to determine the most suitable isotherm model, it is imperative to take into account all available data. R^2 values for models proved that, however, Freundlich isotherm is favorable for this adoption but Langmuir isotherm type 1 illustrated the superior performance and compatibility with the experimental data.

3.4. Comparing with Temkin Isotherm

In this section experimental data (Table 3) were analysed using the Temkin isotherm and compatibility of this isotherm for adsorption of methylene blue dye via GO/TiO_2/SiO_2 photocatalyst was evaluated. The findings were presented in Fig. 9. In addition, the constant, parameters and correlation coefficient values of Temkin isotherm were listed in Table 6. It must be noted that the applied temperature for Temkin isotherm calculations was 298.15K. According the computation, correlation coefficient value for Temkin isotherm was 0.9823. The results of this analysis demonstrated that however, the compatibility of Temkin isotherm was more than Freundlich isotherm, but was lower than the Langmuir isotherm type 1 (Hanes- Woolf).

The lower R^2 observed for Temkin isotherm, as compared to the Langmuir isotherm type 1 (Hanes- Woolf) may be attributed to the inherent characteristics of these isotherms. The Temkin isotherm investigates the impact of temperature on adsorption that declines linearly with coverage of the adsorbate and adsorbent. This model is more suitable for temperature sensitive systems while during this study temperature was constant. Thus, Langmuir isotherm type 1 (Hanes-Woolf) exhibited better performance. Furthermore, it is important to acknowledge that the correlation coefficient values for both models were in the same range, indicating that both models were useful for the interpretation and prediction of adsorption.

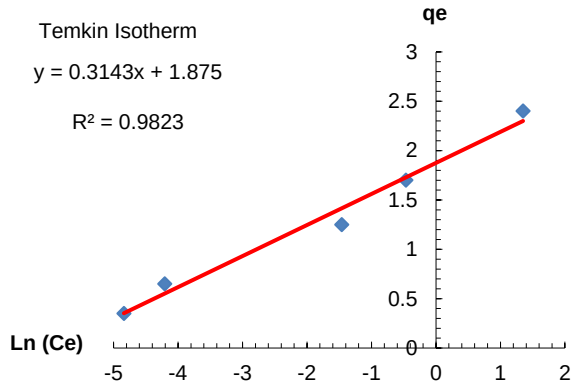

Fig. 9. Temkin isotherm performance for removing of the methylene blue dye.

Table 6. Parameters of Temkin isotherm which was obtained from calculations.

b, J.gr/mol²	K_T, lit/mol	R^2
7886.7932	389.8016	0.9823

Considering the correlation coefficient values for various isotherms, it was observed that the Langmuir isotherm type 1 (Hanes- Woolf with R^2 = 0.9957) exhibited the greatest value, indicating that it is the most suitable model for describing the surface adsorption of methylene blue via the GO/TiO_2/SiO_2 photocatalyst.

3.5. Comparing with Redlich-Peterson, Sips and Toth Isotherms

In this part the adsorption isotherm parameters were defined by applying of non-linear regression analysis. Therefore, experimental outcomes were investigated via utilization of some three-parameter isotherm models such as Redlich-Peterson, Sips and Toth isotherms models. The minimization approach employed in this study involves utilizing the solver add-in function of Microsoft Excel to solve the isotherm. This is achieved by minimizing the hybrid fractional error function (HYBRID) amid the anticipated data and experimental ones.

$$\mathrm{HYBRID} = 100 * \frac{1}{\mathrm{n-p}} * \sum_{i=1}^{n} [(q_{exp} - q_{cal})^2 / (q_{exp})] \qquad (14)$$

Subscripts “exp” and “cal” represent the experimental and calculated q, respectively. Also, n indicates the number of data points. Moreover, p represents the number of parameters in isotherm equation (Shikuku and Jemutai-Kimosop, 2020). The results were exhibited in Fig. 10.

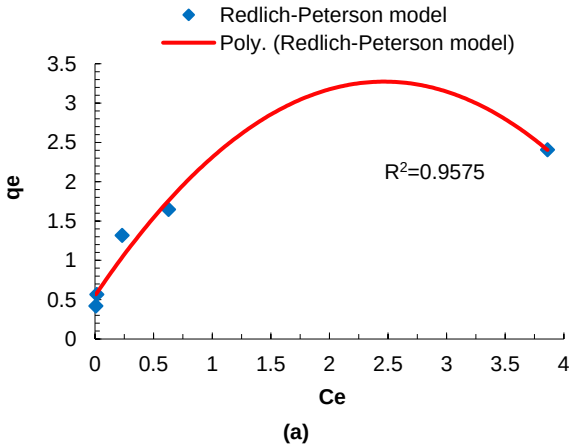

(a)

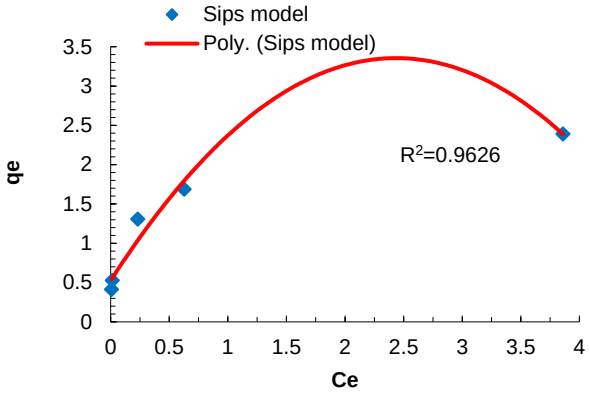

(b)

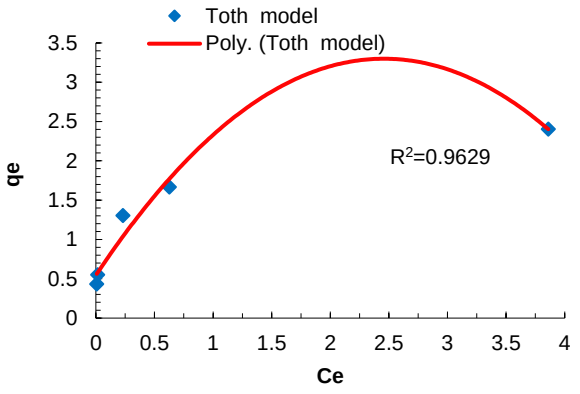

(c)

Fig. 10. (a) Redlich-Peterson, (b) Sips and (c) Toth isotherms models performance for removing of the methylene blue dye.

The constant, parameters and R^2 of isotherms were listed in Table 7. Owing to the calculation, R^2 of Redlich-Peterson, Sips and Toth isotherms models were 0.9575, 0.9626 and 0.9629, respectively. So, it seems that Redlich-Peterson isotherm model illustrated better performance in comparison with other three-parameter models. Comparing the R^2 of Redlich-Peterson, Sips and Toth isotherms with Langmuir isotherm proved that while the Redlich-Peterson model exhibited higher compatibility than the other three-parameter models, it was still lower than the Langmuir isotherm type 1 (Hanes-Woolf). So, we can conclude that, Langmuir isotherm type 1 presented the highest compatibility with experimental data, among the evaluated isotherms.

Table 7. Parameters of Redlich-Peterson, Sips and Toth models which were obtained from the calculations.

Redlich-Peterson model parameters			
K_R (L.g^{-1})	α_R (mg.L^{-1})$^{-\beta}$	β	R^2
132.19	71.649	0.7995	0.9575
Sips model parameters			
q_m	a_s	B_s	R^2
3.6424	1.057	0.4361	0.9626
Toth model parameters			
q_m	a_T	z	R^2
7.0387	0.2737	0.1808	0.9629

4. Conclusions

This study aimed to identify the most suitable isotherm model for the adsorption of methylene blue onto the GO/TiO_2/SiO_2 photocatalyst. Hence, the experimental data obtained from the literature were assessed using various isotherm models, namely Freundlich, Temkin, and three different types of Langmuir isotherms (two-parameter isotherms), as well as Redlich-Peterson, Sips, and Toth models (three-parameter isotherms). Among the different types of Langmuir isotherm models, it was observed that Langmuir isotherm type 1 (Hanes-Woolf) had a significantly high level of performance, as indicated by an R^2 value of 0.9957. Furthermore, upon comparing the results of curve fitting for the two-parameter models, it was seen that the Langmuir isotherm type 1 exhibited the best level of compatibility. Furthermore,

the suitability of Langmuir isotherm to explain the adsorption process was consistent with the computed separation factor (R_L) being in the range of 0 to 1. The major mechanism observed during the adsorption of methylene blue on GO/TiO_2/SiO_2 photocatalyst is likely monolayer adsorption. Additionally, this photocatalyst demonstrated suitability for lower concentrations of methylene blue. Additionally, it can be inferred that the utilization of Temkin isotherms was not suitable for assessing the compatibility of GO/TiO_2/SiO_2 in the degradation of methylene blue in temperature-sensitive systems. The evaluation of three-parameter isotherm models using experimental data demonstrated that the Redlich-Peterson isotherms exhibited greater compatibility when compared to the other models. In general, it can be observed that two-parameter models exhibit greater compatibility and accuracy in predicting adsorption trends compared to three-parameter models. The Langmuir isotherm type 1 is considered the most appropriate model for predicting the adsorption of methylene blue on the GO/TiO_2/SiO_2 photocatalyst, as it exhibits the maximum comparability with experimental results. The obtained results provided valuable insights into the predictive capabilities of the adsorption trend of methylene blue at different concentrations on the GO/TiO_2/SiO_2 photocatalyst. Additionally, these findings presented the opportunities for the development of new photocatalysts for similar applications.

Author Contributions

Seyed Mehdi Sajjadi: Conceptual elucidation, Methodological framework construction, Writing draft of manuscript, Correction of manuscript and editorial and Supervisory role.

Conflict of Interest

The author affirms that he possesses no recognizable conflicting financial affiliations or individual associations that might have appeared to exert an impact on the findings detailed within this manuscript.

Acknowledgements

The author would like to express his deepest gratitude to University of Bonab, Bonab, Iran.

Data Availability Statement

All data used in the article are provided in the text and are available.

References

Abdoli, S. M., Bastani, D. and Bargozin, H. (2015) 'Adsorption of phenol compounds by nanoporous silica aerogel', *Scientia Iranica,* 22(3), pp. 992-1000. Available at: https://scientiairanica.sharif.edu/article_3693.html (Accessesd: 28 October 2023)

Ahmad, H.H., and Alahmad, W. (2021) 'Modeling the removal of methylene blue dye using a graphene oxide/TiO_2/SiO_2 nanocomposite under sunlight irradiation by intelligent system', *Open Chemistry,* 19(1), pp. 157-173. doi: https://doi.org/10.1515/chem-2021-0025

Alahmad, W. A. *et al.* (2018) 'Treatment of simulated wastewater spiked with phenols using TiO_2/GO/SiO_2 under enviromental condition', *Fresenius Environmental Bulletin,* 27, pp. 9922-9930. Available at: https://www.prt-parlar.de/download_feb_2018/ (Accessesd: 28 October 2023)

Bakardjieva, S. *et al.* 'Transformation of brookite-type TiO_2 nanocrystals to rutile: correlation between microstructure and photoactivity', *Journal of Materials Chemistry,* 16(18), pp. 1709-1716. doi: https://doi.org/10.1039/B514632A

Bustos-Terrones, Y. A. *et al.* (2021) 'Removal of BB9 textile dye by biological, physical, chemical, and electrochemical treatments', *Journal of the Taiwan Institute of Chemical Engineers,* 121, pp. 29-37. doi: https://doi.org/10.1016/j.jtice.2021.03.041

Cao, J. *et al.* (2019) 'Decolorization and detoxification of Direct Blue 2B by indigenous bacterial consortium', *Journal of Environmental Management,* 242, pp. 229-237. doi: https://doi.org/10.1016/j.jenvman.2019.04.067

Chakraborty, A. *et al.* (2022) 'TiO_2 nanoflower photocatalysts: Synthesis, modifications and applications in wastewater treatment for removal of emerging organic pollutants', *Environmental Research,* 212, 113550. doi: https://doi.org/10.1016/j.envres.2022.113550

Chiani, E. *et al.* (2020) 'Adsorption of cationic dye from aqueous solution using SBA-15 nano particles synthesized by stem sweep ash as the source of silica', *Journal of Applied Research in Water and Wastewater,* 7(2), pp. 172-179. doi: https://doi.org/10.22126/arww.2021.5648.1186

Chu, K.H. (2021) 'Revisiting the Temkin isotherm: Dimensional inconsistency and approximate forms', *Industrial & Engineering Chemistry Research,* 60(35), pp. 13140-13147. doi: https://doi.org/10.1021/acs.iecr.1c01788

Dada, O. *et al.* (2012) 'Langmuir, freundlich, temkin and dubinin–radushkevich isotherms studies of equilibrium sorption of Zn^{2+} unto phosphoric acid modified rice husk', *IOSR Journal of Applied Chemistry,* 3(1), pp. 38-45. doi: https://doi.org/10.9790/5736-0313845

Demiral, H., and Güngör, C. (2016) 'Adsorption of copper(II) from aqueous solutions on activated carbon prepared from grape bagasse', *Journal of Cleaner Production*, 124, pp. 103-113. doi: https://doi.org/10.1016/j.jclepro.2016.02.084

Ge, J. *et al.* (2019) 'Advanced design and synthesis of composite photocatalysts for the remediation of wastewater: A Review', *Catalysts,* 9(2), 122. doi: https://doi.org/10.3390/catal9020122

Hosseinzadeh, G. *et al.* (2023) 'Synthesis of novel direct Z-scheme heterojunction photocatalyst from WO_3 nanoplates and $SrTiO_3$ nanoparticles with abundant oxygen vacancies', *Surfaces and Interfaces,* 42, 103349. doi: https://doi.org/10.1016/j.surfin.2023.103349

Jegannathan, K. R., and Nielsen, P. H. (2013) 'Environmental assessment of enzyme use in industrial production –a literature review', *Journal of Cleaner Production,* 42, pp. 228-240. doi: https://doi.org/10.1016/j.jclepro.2012.11.005

Joseph, C. G. *et al.* (2021) 'Application of plasmonic metal nanoparticles in TiO_2-SiO_2 composite as an efficient solar-activated photocatalyst: A Review Paper', *Frontiers in Chemistry,* 8, 1283. doi: https://doi.org/10.3389/fchem.2020.568063

Kong, E. D. H. *et al.* (2022) 'GO/TiO_2-related nanocomposites as photocatalysts for pollutant removal in wastewater treatment', *Nanomaterials (Basel),* 12(19), 3536. doi: https://doi.org/10.3390/nano12193536

Li, X. *et al*. (2016) 'Graphene in photocatalysis: A Review', *Small,* 12(48), pp. 6640-6696. doi: https://doi.org/10.1002/smll.201600382

Liu, Y. *et al*. (2009) 'Biosorption of Cd^{2+}, Cu^{2+}, Ni^{2+} and Zn^{2+} ions from aqueous solutions by pretreated biomass of brown algae', *Journal of Hazardous Materials,* 163(2), pp. 931-938. doi: https://doi.org/10.1016/j.jhazmat.2008.07.046

Lu, K.-Q. *et al*. (2021) 'Roles of graphene oxide in heterogeneous photocatalysis', *ACS Materials Au,* 1(1), pp. 37-54. doi: https://doi.org/10.1021/acsmaterialsau.1c00022

Manojkumar, P. *et al*. (2023) 'Development of surface modified titanium alloy as a promising photocatalyst for textile waste water treatment', *Journal of Alloys and Compounds,* 952, 169906. doi: https://doi.org/10.1016/j.jallcom.2023.169906

Mungondori, H. H., and Tichagwa, L. (2013) 'Photo-catalytic activity of carbon/nitrogen doped TiO_2-SiO_2 under UV and visible light irradiation', *Materials Science Forum,* 734, pp. 226-236. doi: https://doi.org/10.4028/www.scientific.net/MSF.734.226

Ncibi, M. C., Mahjoub, B., and Seffen, M. (2007) 'Adsorptive removal of textile reactive dye using Posidonia oceanica (L.) fibrous biomass', *International Journal of Environmental Science & Technology,* 4(4), pp. 433-440. doi: https://doi.org/10.1007/BF03325978

Osmari, T. A. *et al*. (2013) 'Statistical analysis of linear and non-linear regression for the estimation of adsorption isotherm parameters', *Adsorption Science & Technology,* 31(5), pp. 433-458. doi: https://doi.org/10.1260/0263-6174.31.5.433

Parimal, S., Prasad, M., and Bhaskar, U. (2010) 'Prediction of equillibrium sorption isotherm: Comparison of linear and nonlinear methods', *Industrial & Engineering Chemistry Research,* 49(6), pp. 2882-2888. doi: https://doi.org/10.1021/ie9013343

Pei, L. *et al*. (2017) 'Study of hydrolytic kinetics of vinyl sulfone reactive dye in siloxane reverse micro-emulsion', *Textile Research Journal,* 87(19), pp. 2368-2378. doi: https://doi.org/10.1177/0040517516671123

Periyasamy, S. *et al*. (2023) 'Recent advances in consolidated bioprocessing for conversion of lignocellulosic biomass into bioethanol – A review', *Chemical Engineering Journal,* 453, 139783. doi: https://doi.org/10.1016/j.cej.2022.139783

Rabanimehr, F. *et al*. (2021) 'Simulation of photocatalytic degradation of methylene blue in planar microreactor with integrated ZnO nanowires', *Journal of Applied Research in Water and Wastewater,* 8(1), pp. 36-40. doi: https://doi.org/10.22126/arww.2020.4793.1152

Riazian, M. (2014) 'Dependence of photocatalytic activity of TiO_2-SiO_2 nanopowders', *Journal of Nanostructures,* 4(4), pp. 433-441. doi: https://doi.org/10.7508/JNS.2014.04.005

Riazian, M., and Bahari, A. (2012) 'Synthesis and nanostructural investigation of TiO_2 nanorods doped by SiO_2', *Pramana,* 78(2), pp. 319-331. doi: https://doi.org/10.1007/s12043-011-0216-y

Rosales, A., and Esquivel, K. (2020) 'SiO_2@TiO_2 composite synthesis and its hydrophobic applications: A Review', *Catalysts,* 10(2), 171. doi: https://doi.org/10.3390/catal10020171

Safri, A., and Fletcher, A. J. (2023) 'Concentration dependence of TiO_2 nanoparticles in carbon xerogels on adsorption-photodegradation applications', *Gels,* 9(6), 468. doi: https://doi.org/10.3390/gels9060468

Sajjadi, S. M., and Haghighi, M. (2018) 'Impregnation vs. sol-gel and sol-gel-plasma dispersion of nickel nanoparticles over Al_2O_3 employed in combined dry reforming and partial oxidation of greenhouse gases to syngas', *International Journal of Hydrogen Energy,* 43(32), pp. 15014-15029. doi: https://doi.org/10.1016/j.ijhydene.2018.06.073

Sajjadi, S. M., and Haghighi, M. (2019) 'Combustion vs. hybrid sol-gel-plasma surface design of coke-resistant Co-promoted Ni-spinel nanocatalyst used in combined reforming of CH_4/CO_2/O_2 for hydrogen production', *Chemical Engineering Journal,* 362, pp. 767-782. doi: https://doi.org/10.1016/j.cej.2019.01.085

Sajjadi, S. M., Haghighi, M., and Eshghi, J. (2019) 'Synergic influence of potassium loading and plasma-treatment on anti-coke property of K-promoted bimetallic NiCo-$NiAl_2O_4$ nanocatalyst applied in O_2-enhanced dry reforming of CH_4', *International Journal of Hydrogen Energy,* 44(26), pp. 13397-13414. doi: https://doi.org/10.1016/j.ijhydene.2019.03.260

Sajjadi, S. M. *et al*. (2022) 'Plasma-enhanced sol-gel fabrication of CoWNiAl_2O_4 nanocatalyst used in oxidative conversion of greenhouse CH_4/CO_2 gas mixture to H_2/CO', *Journal of CO_2 Utilization,* 61, 102037. doi: https://doi.org/10.1016/j.jcou.2022.102037

Shikuku, V. O., and Jemutai-Kimosop, S. (2020) 'Efficient removal of sulfamethoxazole onto sugarcane bagasse-derived biochar : two and three-parameter isotherms, kinetics and thermodynamics', *South African Journal of Chemistry,* 73(1), pp. 111-119. doi: https://hdl.handle.net/10520/EJC-1f3b0382e4

Shokrolahi, S., Farhadian, M., and Davari, N. (2019) 'Degradation of Enrofloxacin antibiotic in contaminated water by ZnO/Fe_2O_3/Zeolite nanophotocatalyst', *Journal of Applied Research in Water and Wastewater,* 6(2), pp. 150-155. doi: https://doi.org/10.22126/arww.2019.1415

Singh, R. L., Singh, P. K., and Singh, R. P. (2015) 'Enzymatic decolorization and degradation of azo dyes – A review', *International Biodeterioration & Biodegradation,* 104, pp. 21-31. doi: https://doi.org/10.1016/j.ibiod.2015.04.027

Tseng, H.-H. *et al.* (2009) 'Degradation of xylene vapor over Ni-doped TiO_2 photocatalysts prepared by polyol-mediated synthesis', *Chemical Engineering Journal,* 150(1), pp. 160-167. doi: https://doi.org/10.1016/j.cej.2008.12.015

Vargas, A. M. M. *et al.* (2011) 'Adsorption of methylene blue on activated carbon produced from flamboyant pods (Delonix regia): Study of adsorption isotherms and kinetic models', *Chemical Engineering Journal,* 168(2), pp. 722-730. doi: https://doi.org/10.1016/j.cej.2011.01.067

Wang, N. *et al.* (2019) 'Removal of methylene blue by Polyaniline/TiO_2 hydrate: Adsorption kinetic, isotherm and mechanism studies', *Powder Technology,* 347, pp. 93-102. doi: https://doi.org/10.1016/j.powtec.2019.02.049

Zarrabi, M., Haghighi, M., and Alizadeh, R. (2018) 'Sonoprecipitation dispersion of ZnO nanoparticles over graphene oxide used in photocatalytic degradation of methylene blue in aqueous solution: Influence of irradiation time and power', *Ultrasonics Sonochemistry,* 48, pp. 370-382. doi: https://doi.org/10.1016/j.ultsonch.2018.05.034